Modules in connectomes of phase-synchronization comprise anatomically contiguous, functionally related regions

Williams N[1,4], Wang SH[2,3,4], Arnulfo G[2,5], Nobili L[6,7,8], Palva S[2,9,10], Palva JM[2,4,10]

Affiliations:

1. Helsinki Institute of Information Technology, Department of Computer Science, Aalto University, Finland
2. Neuroscience Center, Helsinki Institute of Life Science, University of Helsinki, Finland
3. Doctoral Programme Brain & Mind, University of Helsinki, Finland
4. Department of Neuroscience & Biomedical Engineering, Aalto University, Finland
5. Dept. of Informatics, Bioengineering, Robotics & Systems Engineering, University of Genoa, Italy
6. Claudio Munari Epilepsy Surgery Centre, Niguarda Hospital, Milan, Italy
7. Department of Neurosciences, Rehabilitation, Ophthamology, Genetics and Maternal and Children's Sciences, University of Genoa, Genoa, Italy
8. Child Neuropsychiatry, IRCCs Gaslini Istituto Giannina Gaslini, Genoa, Italy
9. BioMag laboratory, HUS Medical Imaging Centre, Helsinki, Finland
10. Centre for Cognitive Neuroimaging, Institute of Neuroscience & Psychology, University of Glasgow, United Kingdom

Corresponding author:
Dr. Nitin Williams
Department of Computer Science
Aalto University
Konemiehentie 2
02150, Espoo
Helsinki
Tel: +358 (0)44 919 5512
Email: nitin.williams@aalto.fi

Abstract

Modules in brain connectomes are essential to balancing the functional segregation and integration crucial to brain operation. Connectomes are the set of structural or functional connections between each pair of brain regions. Non-invasive methodologies, Electroencephalography (EEG) and Magnetoencephalography (MEG), have been used to identify modules in connectomes of phase-synchronization, but have been compromised by spurious phase-synchronization due to EEG volume conduction or MEG field spread. In this study, we used invasive, intracerebral recordings with stereo-electroencephalography (SEEG, $N = 67$), to identify modules in connectomes of phase-synchronization. To do this, we used submillimetre localization of SEEG contacts and closest-white-matter referencing, to generate group-level connectomes of phase-synchronization minimally affected by volume conduction. Then, we employed community detection methods together with a novel consensus clustering approach, to identify modules in connectomes of phase-synchronization. The connectomes of phase-synchronization possessed significant modular organization at multiple spatial scales, from 3–320 Hz. These identified modules were highly similar within neurophysiologically meaningful frequency bands. Modules up to the high-gamma frequency band comprised only anatomically contiguous regions, unlike modules identified with functional Magnetic Resonance Imaging (fMRI). Strikingly, the identified modules comprised cortical regions involved in shared repertoires of cognitive functions including vision, language and attention. These results demonstrate the viability of combining SEEG with advanced methods, to identify modules in connectomes of phase-synchronization. The modules correspond to brain systems with specific functional roles in perceptual, cognitive, and motor processing.

Keywords

Functional connectome; Phase-synchronization; Stereo-electroencephalography; Brain network modules; Resting-state; Functional systems

Highlights

- SEEG recordings from large cohort used to generate connectomes of phase-synchronization
- Connectomes of phase-synchronization possess modules at multiple spatial scales
- Modules are highly similar within neurophysiologically meaningful frequency bands
- Modules comprise anatomically contiguous regions up to high gamma frequencies
- Modules comprise functionally related regions, suggesting their behavioural relevance

1. Introduction

Structural and functional connectomes obtained from resting-state functional Magnetic Resonance Imaging (fMRI) possess a modular organization (Meunier et al. (2009), Power et al. (2011), Doucet et al. (2011)). Connectomes are the set of connections between each pair of brain regions. Modules are sets of regions with strong connections within modules and weaker connections between them. Modules identified in resting-state fMRI comprise regions that have also been observed to be concurrently active during task processing, and have been found to delineate functional systems for executive, attentional, sensory, and motor processing (Beckmann et al. (2005), Smith et al. (2009), Yeo et al. (2011)). The anatomical structure of resting-state modules in fMRI connectomes has been found to be reproducible and similarly observable with different approaches such as community detection (Valencia et al. (2009), Power et al. (2011)) and clustering (Benjaminsson et al. (2010), Yeo et al. (2011), Lee et al. (2012)). Moreover, the balance between segregated information processing in modules (Wig (2017)) and integrated information processing via inter-modular connections, is essential to brain functioning (Tononi et al. (1994), Tononi et al. (1998), Deco et al. (2015)).

The relationship of fMRI functional connectivity to underlying electrophysiological connectivity is complex and not attributable to any single form of neuronal activity or coupling (Kucyi et al. (2018)). Electrophysiological measurements of macro-scale neuronal activity with Magneto- (MEG) and Electroencephalography (EEG) reveal band-limited neuronal oscillations in multiple frequencies, whose inter-regional coupling is observable as synchronization between oscillation phases and correlations between oscillation amplitude envelopes (Palva et al. (2005), Fell & Axmacher (2011), Brookes et al. (2011), Palva & Palva (2012), Engel et al. (2013)). Amplitude correlations reflect, e.g., co-modulation in neuronal excitability (Vanhatalo et al. (2004), Schroeder & Lakatos (2009), Engel et al. (2013)) while phase-synchronization implies spike-time relationships of neuronal activity and may regulate inter-regional neuronal communication (Fries (2015), Bastos (2015)). Large-scale networks of phase-synchronization are proposed to support the coordination, regulation, and integration of neuronal processing in cognitive functions, both in frequencies up to 130 Hz (Varela (2001), Palva et al. (2005), Uhlhaas et al. (2010), Kitzbichler et al. (2011), Palva & Palva (2012)), and in frequencies higher than 130 Hz, i.e. high-frequency oscillations (HFO) (Arnulfo et al. (2020)).

In light of such putative mechanistic roles for phase synchronization in cognitive functions, a modular architecture and inter-modular coupling in connectomes of phase-synchronization during resting-state, would establish a baseline to support corresponding demands for functional segregation and

integration during cognitive operations (Smith et al. (2009), Spadone et al. (2015)). A single MEG study investigated modules in connectomes of phase-synchronization and amplitude correlation using source-reconstructed resting-state data (Zhigalov et al. (2017)). Both connectomes of amplitude correlation and phase-synchronization comprised distinct modules in frontal regions, sensori-motor regions and occipital regions, particularly in the alpha (8 – 14 Hz) and beta (14 – 30 Hz) frequency bands. However, identifying modules in MEG/EEG connectomes is hindered by errors in estimating the connectome, including false positive connections due to linear mixing from MEG field spread or EEG volume conduction (Palva & Palva (2012), Palva et. al (2018)) or false negatives due to linear-mixing insensitive measures that ignore also true near-zero-lag phase-synchronization (Vinck et al. (2011), Brookes et al. (2012), Palva & Palva (2012)). Low-resolution cortical parcellations that eliminate spurious connections due to linear mixing (Vidaurre et al. (2018)) may be too coarse to identify fine-grained cortical network structures such as modules.

In this study, we pooled resting-state stereo-EEG (SEEG) recordings data from a large cohort (N = 67) to accurately estimate connectomes of phase-synchronization. In contrast to the centimetre-scale, macro-scale insight yielded by MEG, SEEG provides a millimetre range, meso-scale measurement of human cortical local field potentials (LFPs) (Parvizi & Kastner (2018), Zhigalov et al. (2015), Zhigalov et al. (2017)). We combined submillimetre-accurate anatomical localization of SEEG electrode contacts (Narrizano et al. (2017), Arnulfo et al. (2015b)) with a state-of-the-art scheme of referencing each gray-matter contact to its closest white-matter contact (Arnulfo et al. (2015a)), to yield phase-undistorted and polarity-correct measurements of local cortical activity. Crucially, this enabled estimating a high proportion of connections in the connectome while adequately controlling for volume conduction so that near zero-lag phase-synchronization was also measurable (Arnulfo et al. (2015a)). Finally, we used community detection with a novel consensus clustering approach to identify modules in connectomes of phase-synchronization while accounting for missing connections.

We found that connectomes of phase synchronization indeed exhibited modular organization at multiple spatial scales, throughout the studied range of frequencies from 3 to 320 Hz. These modules were highly similar within neurophysiologically meaningful frequency bands and comprised anatomically contiguous regions up to the high-gamma frequency band (80-113 Hz). Strikingly, the modules comprised cortical regions exhibiting shared involvement in specific cognitive functions such as vision, language and attention, suggesting that these modules correspond to brain systems with functional roles in perceptual, cognitive and motor processing.

2. Materials & Methods

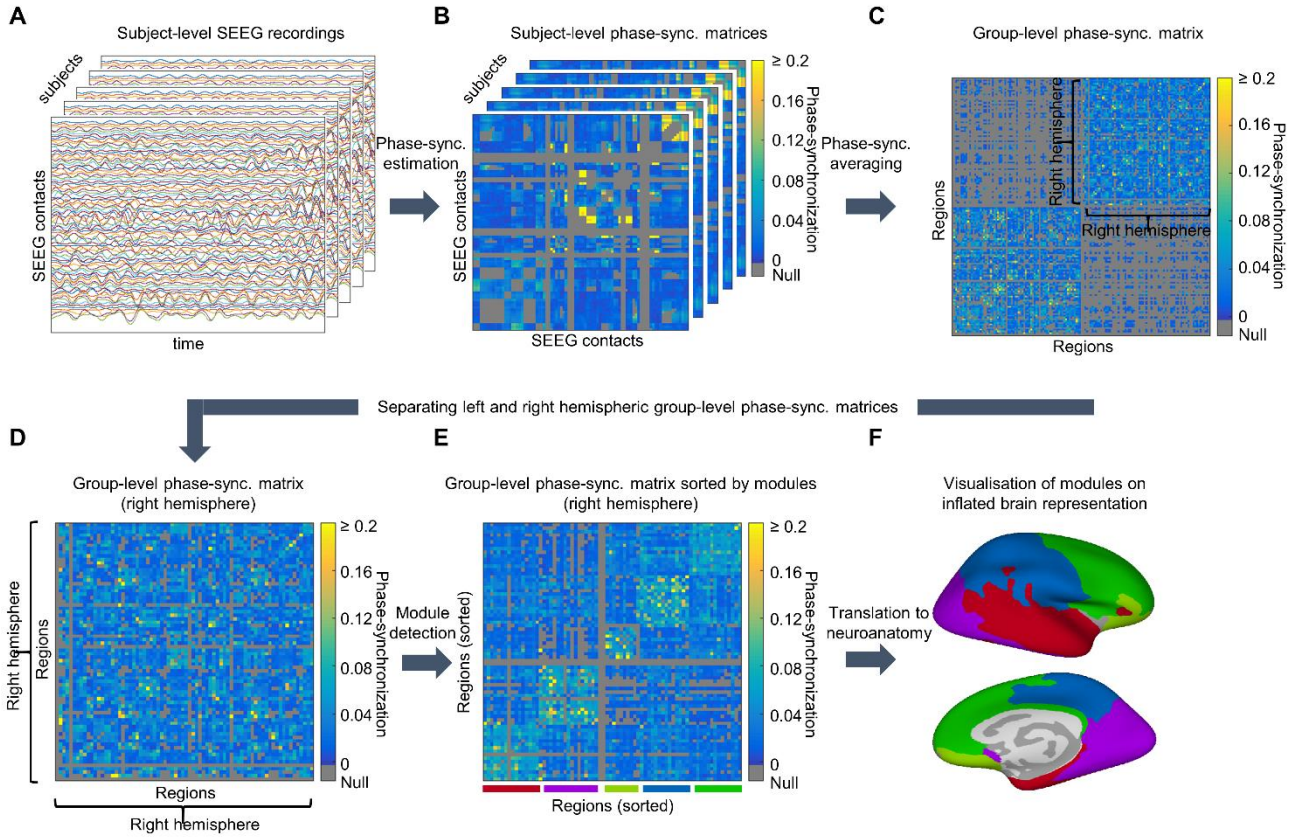

Figure 1. Modules in connectomes of phase-synchronization estimated by pooling data across subjects. A. Band-pass filtered data (centre frequency=14 Hz) for example group of subjects. **B.** Subject-level matrices of phase-synchronization between SEEG contacts, for example group of subjects. **C.** Group-level matrix of phase-synchronization between brain regions. Matrix ordered to show left- (bottom left), right- (top right) and inter-hemispheric connections (top left and bottom right) respectively. Non-estimable connections are gray. **D.** Group-level matrix of phase-synchronization between right-hemispheric regions. **E.** Sorted group-level matrix of phase-synchronization between right-hemispheric regions, sorting done from results of community detection to identify modules. **F.** Colour-coded modules for lateral (top) and medial (bottom) inflated view representation of right hemisphere.

2.1 Analysis pipeline to identify modules in connectomes of phase-synchronization

We combined pre-surgical SEEG recordings from epileptic patients with state-of-the-art methods, to identify modules in connectomes of phase-synchronization. Concretely, we recorded resting-state LFP data from each patient using a common reference in white matter, distant from the putative epileptogenic zone. We re-referenced the LFP activity of each grey-matter SEEG contact to its closest white-matter contact, which we have demonstrated to preserve undistorted phase reconstruction while minimising volume conduction (Arnulfo et al. (2015a)). We filtered the recorded LFP data using 18 narrow-band Finite Impulse Response (FIR) filters (Figure 1A) from 2.5 Hz up to 350 Hz with line-

noise suppressed using band-stop filters at 50Hz and harmonics. Next, we estimated the strength of phase synchronization between every pair of SEEG contacts, for each frequency, using Phase Locking Value (PLV) (Figure 1B). We assigned cortical SEEG contacts to brain regions using an automated submillimeter-accurate electrode localization procedure involving CT-MRI co-localization (Arnulfo et al. (2015b)). We then estimated group-level connectomes by averaging for each region-pair, the corresponding contact-contact PLVs across subjects (Figure 1C). We analyzed the left and right hemispheres separately (Figure 1D) and identified modules with Louvain community detection (Blondel et al. (2008)) combined with consensus clustering (Williams et al. (2019)) (Figure 1E). Finally, we visualised the identified modules on anatomical brain surfaces (Figure 1F).

2.2 Data acquisition

We recorded SEEG data from 67 participants affected by drug-resistant focal epilepsy and undergoing pre-surgical clinical assessment. For each participant, we inserted 17 ± 3 (mean ± SD) SEEG shafts into the brain, with anatomical positions varying by surgical requirements. Each shaft had between 8 and 15 platinum-iridium contacts, each contact being 2 mm long and 0.8 mm thick, with inter-contact distance of 1.5 mm (DIXI medical, Besancon, France). We acquired 10 minutes eyes-closed resting-state activity from each participant, via a 192-channel SEEG amplifier system (Nihon Kohden Neurofax-110) at a sampling frequency of 1 kHz. We obtained written informed consent from participants prior to recordings. We obtained ethics approval for the study from Niguarda "Ca' Granda" Hospital, Milan, and we performed the study according to WMA Declaration of Helsinki – Ethical Principles for Medical Research Involving Human Subjects.

2.3 Pre-processing

We performed re-referencing, filtering and artefact removal of the SEEG data, before estimating the connectome of phase-synchronization. We originally recorded data from all contacts with a monopolar referencing scheme. We subsequently re-referenced activity from each gray-matter contact to the nearest white matter contact as identified by GMPI (gray matter proximity index). We have previously demonstrated the utility of this referencing scheme in studying phase synchronization, since phase relationships between contacts are well preserved (Arnulfo et al. (2015a)). We only analysed activity from gray-matter contacts after re-referencing. We filtered activity from each gray-matter contact using FIR filters (equiripples 1% of maximal band-pass ripples) into 18 frequency bands, with center frequencies (F_c) ranging from 3 to 320 Hz (excluding 50 Hz line-noise and harmonics). We used center frequencies of 3 Hz, 4 Hz, 5 Hz, 7 Hz, 10 Hz, 14

Hz, 20 Hz, 28 Hz, 40 Hz, 57 Hz, 80 Hz, 113 Hz, 135 Hz, 160 Hz, 190 Hz, 226 Hz, 269 Hz and 320 Hz. We used a relative bandwidth approach for filter banks such that pass band (W_p) and stop band (W_s) were defined $0.5 \times F_c$ and $2 \times F_c$, respectively for low and high-pass filters. Before estimating phase synchronization, we excluded selected windows of data due to artefactual epileptic activity. Specifically, we discarded 500 ms wide windows containing Inter-Ictal Epileptic (IIE) events. We defined IIE as at least 10 % of SEEG contacts narrow-band time series demonstrating abnormal, concurrent sharp peaks in more than half the 18 frequencies. To identify such periods, we searched for "spiky" periods in amplitude envelopes of each SEEG contact. We tagged a 500 ms window as "spiky" if any of its samples were 5 standard deviations higher than mean amplitude of the contact.

2.4 Connectome estimation

We pooled estimates of phase-synchronization between SEEG contacts to obtain the group-level connectome of phase-synchronization. We measured phase synchronization between SEEG contacts with Phase Locking Value (PLV) (Lachaux et al. 1999):

$$PLV = \frac{1}{N}\left|\sum_{n=1}^{N} e^{j(\theta_1(n)-\theta_2(n))}\right|$$

where $\theta_1(n)$ and $\theta_2(n)$ are instantaneous phases from a pair of SEEG contacts at sample n, with N being the total number of samples. To estimate the connectome of phase synchronization at the group-level, we first selected a brain atlas for dividing the brain into a number of regions. We used the 148-region Destrieux brain parcellation (Destrieux et al. (2010)). We determined phase synchronization between a pair of brain regions by averaging PLV over all subjects, for all contact-pairs traversing that pair of brain regions. We localised each SEEG contact to brain regions using the automated procedure we validated in Arnulfo et al. (2015b). Once we estimated the connectome, we retained the estimated strengths of only the top 20 percentile of connections, setting all others to 0.

Since we did not have complete recording coverage of the brain with SEEG, we had insufficient data to estimate phase synchronization between all region-pairs. In all, we obtained estimates for 47.2% of all region-pairs. A high proportion of inter-hemispheric connections were not estimable since SEEG contacts are typically concentrated in a single hemisphere for a given subject.

We excluded selected contact-pairs from the connectome estimation due to potential artefacts. Concretely, we excluded contact-pairs with epileptogenic contacts. Further, we excluded contact-

pairs whose respective SEEG contacts were less than 20 mm apart and those with the same white-matter reference, both to reduce the effect of volume conduction.

2.5 Analysing the connectome of phase synchronization

2.5.1 Identifying modules in connectomes of phase synchronization

We used Louvain community detection (Reichardt & Bornholdt (2006), Blondel et al. (2008), Ronhovde & Nussinov (2009), Sun et al. (2008)) combined with consensus clustering (Lancichinetti & Fortunato (2012)) to identify modules in the connectome of phase-synchronization. We used the implementation of the Louvain method in Brain Connectivity Toolbox (Rubinov & Sporns (2010)). We applied the Louvain method to left and right hemispheric regions separately, since the low number of inter-hemispheric connections might confound the identification of modules. To identify modules while accounting for missing values in the group-level connectome matrix, we first generated 5000 variants of the connectome wherein we replaced each missing value with a randomly selected existing value. We applied Louvain community detection to identify modules on each of these 5000 complete matrices. We identified modules at a range of spatial scales by setting the γ input parameter of the Louvain method from 0.8 to 5, in intervals of 0.1. For each γ value, we combined the module assignments of the 5000 connectome variants to obtain a consensus module assignment. We performed this step by first generating matrix representations of each module assignment, with number of matrix rows and columns being the number of regions. We set each element in the matrix to 1 or 0 depending respectively on whether that pair of regions were in the same module or not. We then obtained a consensus matrix by averaging the 5000 matrix representations, and obtained a consensus module assignment by applying the Louvain method to this consensus matrix. We have demonstrated this consensus clustering approach is superior to other approaches to identify modules in incomplete human brain networks (Williams et al. (2019)). We applied this procedure to identify modules at each frequency, for left and right hemispheres separately.

2.5.2. Determining statistical significance of modular organization

We determined statistical significance of modular organization by comparing modularity of connectomes against modularity of randomized versions of the connectome. Modularity is the extent to which the connectome divides into non-overlapping modules. We first estimated modularity of the connectome for γ values (spatial scales) from 0.8 to 5 when identifying modules, using the same procedure described in Section 2.5.1. Modularity is returned as an output of Louvain community detection. We used 100 connectome variants for the consensus clustering step. At each γ value, we

then z-scored the estimated modularity against a null distribution of 100 modularity values obtained by identifying modules on randomly rewired (without replacement) versions of the original connectome, where we performed rewiring the same way for each connectome variant in the consensus clustering step. We estimated z-scored modularity for each frequency, for left and right hemispheres separately. We then converted the z-scores to p-values assuming a Gaussian distribution, and used False Discovery Rate (FDR) thresholding (Benjamini & Hochberg (1995)) to correct for multiple comparisons, to assess modular organization for every combination of γ and frequency. We considered FDR-corrected $p < 0.05$ to indicate statistically significant modular organization.

2.5.3 Determining statistical significance of percentage of stable regions

We determined stability of module assignment for each brain region by the extent to which module affiliations in bootstrapped versions of the original connectome matched those in the original connectome. We constructed 100 bootstrapped connectomes with the same procedure used for the original connectome, but from a set of 67 subjects randomly resampled (with replacement) from the original cohort. We estimated the stability of module assignment of a region as the average correspondence in its module affiliation, with module affiliations of the same region across the 100 bootstrapped connectomes. We specified the module affiliation vector of a region to contain '1' for regions in the same module and '0' for regions in different modules. We estimated the correspondence between two module affiliation vectors by the total number of common '1's and '0's as a proportion of the number of regions. Values close to 1 reflected stable assignment of a region to its module. We estimated the percentage of regions whose module assignments were stable, where regions were considered to have stable module assignment if their stability was higher than the 95-percentile value of the null distribution of stability values. We generated the null distribution of stability values for each region, by estimating average correspondence between its module affiliation vector and 100 randomly resampled (without replacement) module affiliation vectors of the same region, for each of the bootstrapped connectomes. We estimated the percentage of stable regions for each combination of spatial scales or γ values (from 0.8 to 5) and frequencies, for both left and right hemispheres. We determined the statistical significance of the percentage of stable regions, by z-scoring it against the percentage of regions assigned as stable by chance. We then converted the z-scores to p-values assuming a Gaussian distribution, and used False Discovery Rate (FDR) thresholding to correct for multiple comparisons due to testing across every combination of γ and frequency. We considered FDR-corrected $p < 0.05$ to indicate statistically significant percentage of stable regions.

2.5.4. Grouping frequencies by similarity of modules

We used multi-slice community detection (Mucha et al. (2010)) to identify groups of frequencies with similar modules, simultaneously for both left and right hemispheres. First, we generated matrices of similarity between modules at each pair of frequencies, separately for left and right hemispheres. We generated matrix representations of modules at each frequency with number of rows and columns equal to the number of brain regions, each element being set to 1 or 0 depending respectively on whether the corresponding pair of brain regions were in the same module or not. We measured similarity between modules using partition similarity (Ben-Hur et al. (2002)):

$$PS = \frac{\langle l1, l2 \rangle}{\sqrt{\langle l1, l1 \rangle \langle l2, l2 \rangle}}$$

where $\langle lm, ln \rangle = \sum_{i,j} C_{i,j}^{(m)} C_{i,j}^{(n)}$, *i.e.* the dot product between matrix representations of the modules for frequencies m and n. We obtained matrices of partition similarity for each γ value (spatial scale) from 0.8 to 5 and combined them via a weighted average, where we specified the weights as the number of frequencies for which modular organization was statistically significant at each γ.

We entered these left and right hemispheric matrices of module similarity into a multi-slice community detection procedure, to identify groups of frequencies with similar modules for both hemispheres. This method has two input parameters, $\gamma_{\text{multislice}}$ and ω. $\gamma_{\text{multislice}}$ influences the number of identified groups of frequencies while ω controls the dependence between the identified groups of left and right hemispheres. To select values for these parameters, we first estimated modularity values for each combination of $\gamma_{\text{multislice}} = 1 - 1.5$ (intervals of 0.05) and $\omega = 0.1 - 1$ (intervals of 0.1). Then, we generated a null distribution of modularity values by applying the method to identically randomly resampled (without replacement) left and right hemispheric matrices of module similarity. We *z*-scored the original modularity values against the null distribution, and converted them to *p*-values assuming a Gaussian distribution. Finally, we inspected frequency groups for selected combinations of $\gamma_{\text{multislice}}$ and ω with FDR-thresholded $p < 0.05$.

2.5.5 Identifying modules across multiple frequencies or spatial scales

We used a consensus clustering approach (Section 2.5.1) to identify a single set of modules across a group of frequencies. Concretely, we first averaged matrix representations of modules at individual frequencies and applied Louvain method to identify modules in this averaged matrix. Matrix representations have number of rows and columns equal to the number of brain regions, each element in the matrix is 1 or 0 depending respectively on whether the corresponding pair of regions are in the

same module or not. We obtained the consensus modules across all investigated frequencies and spatial scales by first generating matrix representations of modules at each individual frequency and spatial scale, for left and right hemispheres separately. Then, we applied multi-slice community detection ($\gamma_{multislice} = 1.6$, $\omega = 1$) to identify eight bilaterally symmetric modules, which represented sets of regions assigned to the same module across frequencies and spatial scales.

2.6 Inferring whether regions in a module are functionally related.

We combined Neurosynth meta-analyses decoding (Yarkoni et al. (2011)) with comparison to surrogate modules, to assign putative functional roles to each module. We used Neurosynth decoding to find terms related to perception, cognition and behaviour selectively associated to the centroid co-ordinates of each brain region, based on a large database of fMRI studies. Then, we aggregated the terms associated to each region in a module and compared the occurrence frequencies of these terms to those of equally sized surrogate modules, which comprised anatomically proximal regions and were constrained to be bilaterally symmetric. Hence, we determined terms that were common to regions in a module, even after accounting for the anatomical proximity of its regions. We *z*-scored the occurrence frequency of each term in a module against corresponding frequencies of the surrogate modules. We converted these *z*-scores to *p*-values assuming a Gaussian distribution and FDR-thresholded at $p < 0.05$, to reveal those terms selectively associated to each module.

We inferred the putative functional role of each module by the set of terms it was selectively associated to. We also performed a post-hoc analysis to verify the functional specificity of each module. To do this, we generated an 8×8 'confusion matrix' of percentages of selectively associated terms of each module distributed across the eight cognitive functions assigned to the modules. High values along the diagonal would reflect high functional specificity, *i.e.* that the terms of each module were largely confined to a single cognitive function. We compared these percentages against the percentages of all terms related to a module, not just those selectively associated to each module. We expected these sets of all terms of each module to be distributed across diverse cognitive functions.

2.7 Assessing robustness of results

We assessed robustness of results, to changes in the SEEG contact-pairs used to generate the connectomes, changes in the algorithm used to identify modules, and the influence of amplitudes of activity from brain regions on estimating modules. First, we identified and compared modules identified from split connectomes at $\gamma = 2$, each of the split connectomes being generated by combining different sets of SEEG contact-pairs. To generate a split connectome, we estimated

strength of each connection from a randomly selected sample of half the SEEG contact-pairs used to estimate strength of each estimated connection in the original connectome. We estimated the same connection in the other split connectome with the other half of SEEG contact-pairs used to estimate strength of that connection in the original connectome. Next, we compared the original modules obtained with Louvain community detection at $\gamma = 2$, against modules obtained with Infomap community detection (Rosvall & Bergstrom (2008)). Network density influences the number of modules with Infomap - we set the network density to 10% since this value yielded interpretable modules in previous work (Williams et al. (2019)). Finally, we investigated if identifying modules is confounded by amplitude of oscillations from individual nodes in a network. To do this, we compared modules of 20 subject-level networks of phase synchronization before and after removing amplitude-related differences in functional connection strengths, at $\gamma = 2$. We removed amplitude-related differences by relating the strengths of each functional connection to average amplitude of corresponding node-pairs via linear regression, and recovering the residuals. We compared modules identified before and after removing amplitude-related differences with partition similarity.

3. Results

In this study, we pooled SEEG recordings from a large cohort to estimate connectomes of phase-synchronization at multiple frequencies, and applied Louvain community detection together with consensus clustering to identify modules in these connectomes. We used permutation-based and bootstrap-based tests to determine the range of spatial scales with significant modular organization. Further, we used multi-slice community detection to determine groups of frequencies with highly similar modules. Finally, we extended meta-analysis-based decoding of single brain regions to determine if regions within each module were involved in the same cognitive functions.

3.1 Whole-brain coverage achieved by broad spatial sampling of SEEG contacts

We assessed coverage of SEEG contacts across participants, to determine their sampling of brain regions and inter-regional connections. We quantified sampling of brain regions and inter-regional connections by the percentage of brain regions and region-pairs in Destrieux brain atlas (Destrieux et al. (2010)) containing at least one SEEG contact or contact-pair, respectively. We also estimated number of SEEG contacts in each of the Yeo functional systems (Yeo et al. (2011)). Our cohort sampled with at least one SEEG contact, 97% of brain regions (143 of 148) in the Destrieux brain atlas (Figure 2A). The SEEG contacts were sampled more densely on the right ($N = 45 \pm 38$, mean ±

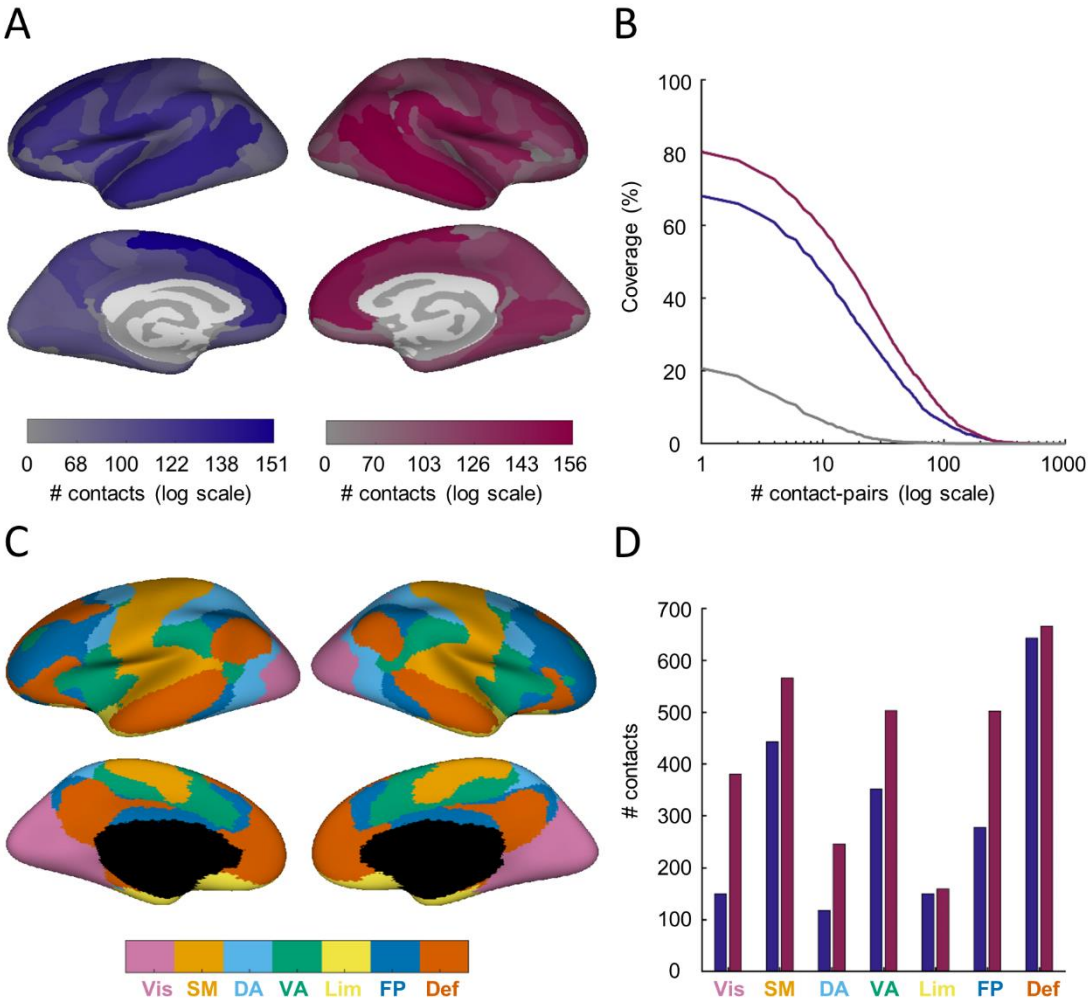

Figure 2. Whole-brain coverage achieved by placement of SEEG contacts. A. Number of SEEG contacts in each brain region for left (dark blue) and right (dark red) hemispheres, from lateral (top) and medial (bottom) views. **B.** Coverage of left-hemispheric (dark blue), right-hemispheric (dark red) and inter-hemispheric (gray) connections for a range of minimum number of SEEG contact-pairs. **C.** 7 Yeo systems from lateral (top) and medial (bottom) views. VIS = Visual, SM = Sensori-motor, DA = Dorsal Attention, VA = Ventral Attention, Lim = Limbic, FP = Fronto-parietal and Def = Default Mode. **D.** Number of SEEG contacts in each of 7 Yeo systems, for left (dark blue) and right (dark red) hemispheres.

standard deviation, range 0-123, contacts per subject) than the left (32 ± 41, 0-128, contacts per subject) hemisphere. This yielded a coverage of 68% of left-hemispheric, 80% of right-hemispheric connections and 20% of inter-hemispheric connections (Figure 1B). Further, the SEEG contacts densely sampled each of the 7 Yeo functional systems (Figure 1C, D). Hence, we achieved whole-brain coverage due to the broad sampling of SEEG contacts across participants.

3.2 Connectomes of phase-synchronization possess modules at multiple spatial scales

Statistical significance of the identified modules would suggest that these modules operate as functional systems within the connectome. Hence, we determined the statistical significance of the identified modules and further, if they were statistically significant at a single spatial scale or at multiple spatial scales. Networks with modules at multiple spatial scales have qualitatively different dynamics to networks with modules at a single spatial scale, for *e.g.* having characteristic time scales and temporal evolution of synchronization (Arenas et al. (2006)). We used Louvain community detection with a range of the γ parameter from 0.8 to 5 to identify modules at multiple spatial scales. The numbers of modules varied from 1 to 18 across the range of spatial scales and frequencies (Figure 3A). We used bootstrap- and permutation-based methods to assess statistical significance of the identified modules. The permutation method operated on the entire connectome while the bootstrap method operated on individual regions, hence the permutation method is a more conservative test of modular organization. In the bootstrap method, we determined if the percentage of brain regions consistently assigned to the same module across bootstrapped versions (N = 100) of the original connectome, was more than would be expected by chance. In the permutation method, we assessed if modularity of the original connectome was higher than modularity of ensembles of randomized versions of the connectome (N = 100). Modularity is the extent to which the connectome divides into non-overlapping modules. We observed that across a wide range of spatial scales and frequencies, 12.2–100% cortical regions had stable module assignments, yielding statistically significant percentages of stable regions at multiple spatial scales ($p < 0.05$, FDR-corrected, bootstrap test) (Figure 3B). Further, the connectomes had statistically significant modular organization ($p < 0.05$, FDR-corrected, permutation test) at multiple spatial scales throughout the studied frequency range (Figure 3C). Connectomes in beta frequency band (14-20 Hz) exhibited the widest range of spatial scales for which modules were statistically significant. The statistical significance of the modules suggests that they operate as functional systems within the connectome, and their existence at multiple spatial scales influences the nature of dynamics from the connectome, for *e.g.* characterised by a range of temporal scales.

For a given frequency, we displayed modules on projections of the cortical surface (Figure 3D). At a representative frequency of 14 Hz, modules comprised superior-frontal, inferior-frontal, temporal, parietal and occipital regions at a coarse spatial scale (γ = 1.8). The module of temporal regions split into modules of superior and inferior-temporal regions at finer spatial scales (γ = 2.6) (Figure 3E).

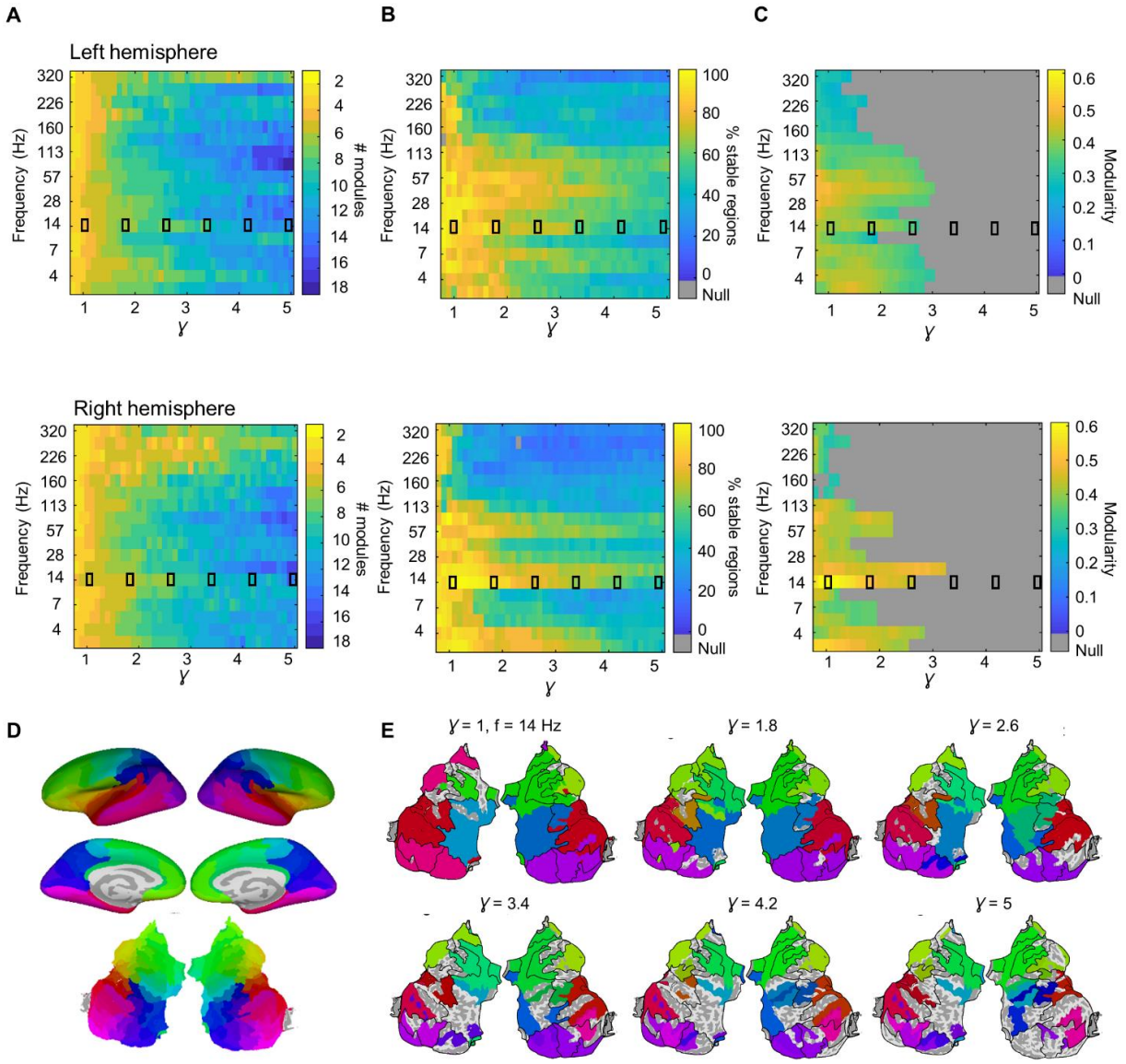

Figure 3. Connectomes of phase-synchronization are modular at multiple spatial scales. **A.** Number of identified left and right hemisphere modules, for each combination of spatial scale and frequency. **B.** Percentage of left and right hemisphere regions with stable module assignments, for each combination of spatial scale and frequency. **C.** Modularity measure for left and right hemisphere, for each combination of spatial scale and frequency. Modularity values below statistical significance are gray. **D.** Translation of colours for each brain region from an inflated-brain (top) to a flat-brain representation (bottom). Colour of each region is a function of distance and angle from the centre of the flat-brain, such that neighbouring regions are coloured similarly. **E.** Colour-coded modules for right hemisphere at 14 Hz on flat-brain representation, at six spatial scales (γ = 1 to 5). Module colours reflect anatomical location of their constituent regions, since they are obtained from the mean angles and distances from centre of these regions. Regions with unstable module assignments are gray.

424

3.3 Modules in connectomes of phase synchronization group into neurophysiologically meaningful frequency bands

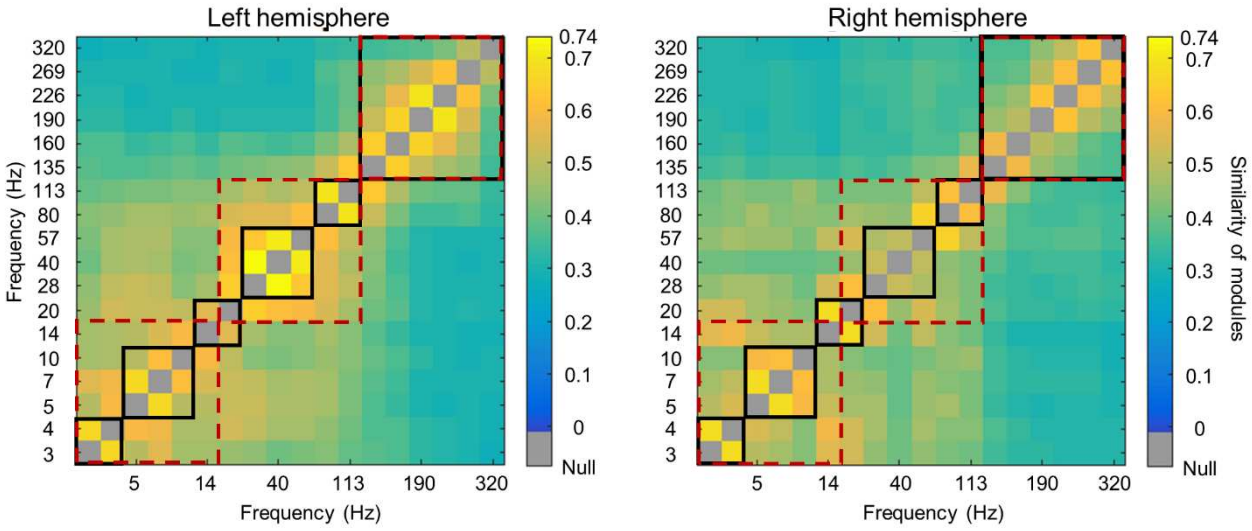

Figure 4. Modules in connectomes of phase-synchronization group into neurophysiologically meaningful frequency bands. Matrices of similarity between modules in connectomes of phase-synchronization for every pair of frequencies, for left and right hemispheres. Statistically significant grouping for both hemispheres into three frequency bands (dashed red outline), *i.e.* 3-14 Hz, 20-113 Hz and 135-320 Hz and six frequency bands (black outline), *i.e.* 3-4 Hz, 5-10 Hz, 14-20 Hz, 28-57 Hz, 80-113 Hz and 135-320 Hz, are shown.

We determined if the identified modules group into statistically distinct sets of frequencies. To do this, we generated matrices of similarity between modules for every pair of frequencies, and applied multi-slice community detection (Mucha et al. (2010)) to identify bilaterally symmetric frequency bands within which modules were highly similar (Figure 4). We found multiple statistically significant ($p < 0.05$, FDR-corrected, permutation test, $N = 100$) groupings of between two and thirteen frequency bands. For further analysis, we used the groupings into three frequency bands and six frequency bands, though we note that other equally valid groupings could be used. The statistically significant grouping into three frequency bands ($\gamma = 1.1$, $\omega = 0.2 - 1$) comprised sets of adjacent frequencies, 3–14 Hz, 20–113 Hz and 135–320 Hz (Figure 4, dashed red line boxes). Similarly, the statistically significant grouping into six frequency bands ($\gamma = 1.25$, $\omega = 0.2 - 1$) comprised sets of adjacent frequencies, 3–4 Hz, 5–10 Hz, 14–20 Hz, 28–57 Hz, 80–113 Hz and 135–320 Hz (Figure 4, solid black line boxes). Notably, the grouping into six sets of frequencies yielded frequency bands that are close to neurophysiologically meaningful frequency bands observed in prior literature, *i.e.* delta (3-4 Hz), theta/alpha (5-10 Hz), beta (14-20 Hz), low gamma (28-57 Hz), high gamma (80-113

Hz) and high-frequency oscillations (135-320 Hz) respectively (Lopes da Silva (2011), Arnulfo et al. (2020)). Thus, the identified modules group into statistically distinct sets of adjacent frequencies, which map to neurophysiologically meaningful frequency bands.

3.4 Modules in connectomes of phase synchronization comprise anatomically contiguous regions

Module-like structures identified in resting-state fMRI, such as the default mode, fronto-parietal, ventral- and dorsal-attention systems include anatomically non-contiguous regions (van den Heuvel & Pol (2010)). We investigated if modules in connectomes of phase-synchronization similarly comprised anatomically non-contiguous regions for the statistically significant grouping into three and six frequency bands, at different spatial scales (Figure 5). For the grouping into three frequency bands (3–14 Hz, 20–113 Hz and 135–320 Hz), we in fact found the modules comprised only anatomically contiguous regions for the 3–14 Hz and 20–113 Hz frequency bands, where the modules respectively comprised frontal, temporal and parietal regions at a coarse spatial scale ($\gamma = 1$). At finer spatial scales ($\gamma = 2, 3$), the module of temporal regions split into separate modules of superior-temporal and inferior-temporal regions. The module of frontal regions also split into separate modules of superior-frontal and inferior-frontal regions. Similarly, modules of the six frequency bands (3–4 Hz, 5–10 Hz, 14–20 Hz, 28–57 Hz, 80–113 Hz and 135–320 Hz) comprised anatomically contiguous regions up to 113 Hz (Figures S1-2). However, in contrast to modules for the 3–14 Hz and 20–113 Hz frequency bands, and corresponding bands in the grouping into six frequency bands, the modules in the 135–320 Hz frequency band included anatomically non-contiguous regions (Figure 5) (Arnulfo et al. (2020)). Hence, unlike with resting-state fMRI, modules in connectomes of phase-synchronization up to high-gamma frequencies comprised anatomically contiguous regions.

Please find module assignments for left and right hemispheres, at a number of spatial scales ($\gamma = 1, 2, 3, 4$), in our shared open dataset (Williams et al. (2021)).

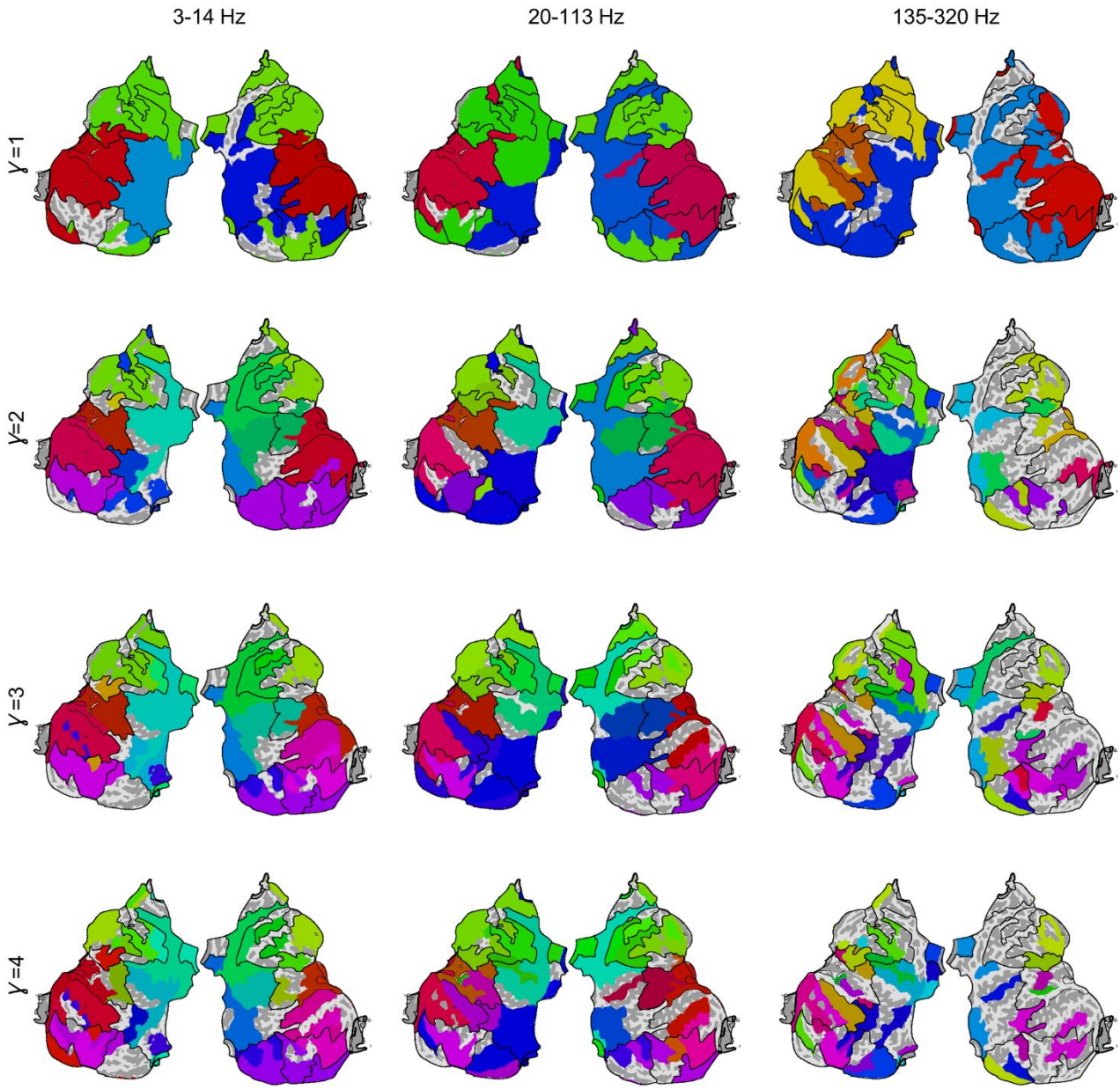

Figure 5. Modules in connectomes of phase-synchronization up to high-gamma frequencies comprise anatomically contiguous regions. Flat-brain representations of modules in connectomes of phase-synchronization for 3-14 Hz, 20-113 Hz and 135-320 Hz, at four spatial scales (γ = 1 to 4). Black lines on each flat-brain show outlines of consensus modules, *i.e.* sets of regions assigned to the same module across frequencies and spatial scales.

3.5 Modules in connectomes of phase synchronization comprise functionally related regions

Module-like structures identified in fMRI comprise regions that are concurrently active in tasks relating to specific sensory, motor, or cognitive domains, such as visual, sensorimotor, attentional, and executive control processing (Smith et al. (2009), Power et al. (2011)). Hence, we investigated if modules in connectomes of phase-synchronization also comprised regions that are concurrently active in tasks relating to specific cognitive domains. For this purpose, we used eight consensus modules that represented sets of regions assigned to the same module across frequencies and spatial scales. In the absence of *a-priori* knowledge on number of consensus modules, we set the number as eight to fall within the range of seven to ten reported for their putative fMRI counterparts (Beckmann et al. (2005), Damoiseaux et al. (2006), Yeo et al. (2011), Power et al. (2011)). The eight consensus modules comprised anatomically contiguous regions and included regions in the superior-frontal (bright green), inferior-frontal (pale green), insula (olive), superior-temporal (brown), inferior-temporal (dark pink), parietal (light blue), lateral-occipital (dark purple), and medial-occipital (light purple) cortical areas (Figure 6A). Module colours reflect anatomical location of their constituent regions. The consensus modules predominantly resembled modules at the lower frequencies (14-40 Hz) and intermediate spatial scales (γ = 1.5–2.5) (Figure S3).

We first used the Neurosynth meta-analyses-based decoding tool (Yarkoni et al. (2011)) to find terms related to perception, cognition and behaviour, selectively associated with each brain region in the Destrieux brain atlas, where we identified each region by its centroid coordinates. These terms were both sensitively and specifically associated to fMRI activation in the corresponding brain regions, according to a large database of fMRI studies. We then identified terms selectively associated with each module by finding terms that occurred more frequently ($p < 0.05$, FDR-corrected, permutation test, $N = 74$) across the regions in a module, compared to equally sized surrogate modules of anatomically contiguous regions. This effectively tested the hypotheses that regions comprising a module serve shared functional roles, even after accounting for their anatomical proximity.

The terms for the superior-frontal module related to attention and executive function while the terms for the inferior-frontal module related to affective processing and social cognition (Figure 6A). The terms for the parietal module related to sensori-motor, sensory and motor processing. In addition, the terms for the modules in the occipital lobe, the medial-occipital and lateral-occipital modules, related to visual processing and the terms for the superior-temporal module related to language and auditory processing. Finally, the terms for the inferior-temporal module related to memory function and the

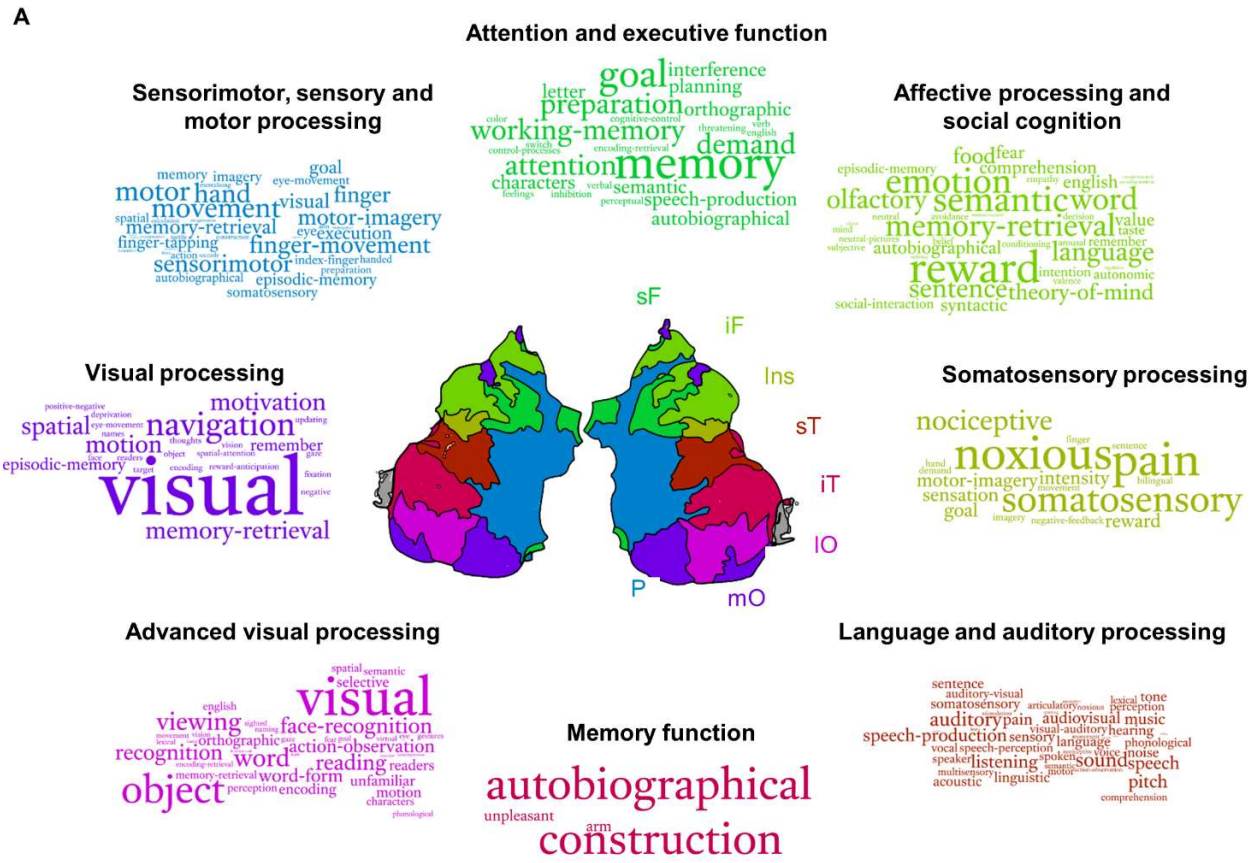

Figure 6. Modules in connectomes of phase-synchronization comprise functionally related regions. A. Terms and putative functional roles specific to each of the eight consensus modules displayed in centre. Sizes of words are proportional to their frequency of occurrence. sF=superior Frontal, iF=inferior Frontal, Ins=Insula, sT=superior Temporal, iT=inferior Temporal, lO=lateral Occipital, mO=medial Occipital, P=Parietal. **B.** Percentages of terms specific to each module (row) assigned to each of eight cognitive functions (left) and percentages of all terms related to each module (row) assigned to the same cognitive functions (right).

terms for the insula module related to somatosensory processing. The results suggest that, similarly to modules in resting-state fMRI, the modules in connectomes of phase-synchronizaton comprised regions with shared functional roles in task-related processing. The putative functional roles of these modules, inferred from their sets of terms, were in good agreement with overarching functions of their constituent regions (Gazzaniga et al. (2009)).

Please find the set of terms selectively associated to each of the consensus modules, in our shared open dataset (Williams et al. (2021)).

We sought further verification of the functional specificity of modules, *i.e.* that they are specialised to support particular cognitive functions rather than support diverse cognitive functions. To verify this, we determined the percentage of selectively associated terms for each module that could be categorised under every module's assigned functional role. We compared this against the percentage of all terms for each module, *i.e.* before FDR-thresholding, that could be categorised under every module's assigned cognitive function. Functional specificity of modules would be reflected by high percentages of selectively associated terms for each module being assigned to their assigned cognitive function, but the set of all terms for each modules being distributed across diverse cognitive functions. As expected, we found high percentages of selectively associated terms for each module were categorised within the cognitive function assigned to them (Figure 6B, left), but the set of all terms for each module were distributed across diverse cognitive functions (Figure 6B, right). These results further verify the functional specificity of the identified modules.

3.6 Robustness of results

We evaluated the robustness of the identified modules to the specific SEEG electrode-contact pairs used to generate the connectomes. To do this, we generated two split connectomes from the original connectome and compared the modules identified from each. Modules identified from the split connectomes were highly similar to each other (Figure S4). Hence, the identified modules were robust to the particular SEEG contact-pairs used to generate the connectomes.

We further evaluated the robustness of the identified modules to the particular algorithm used for community detection. To do this, we identified modules with Infomap community detection (Rosvall & Bergstrom (2008)) and compared these to the modules we had identified with Louvain community detection. Modules identified by both these methods were highly similar up to high-gamma (113 Hz) (Figure S5). Hence, the identified modules were robust to the particular algorithm used up to high-gamma frequencies but were algorithm-specific for high-frequency oscillations (135–320 Hz).

Finally, we investigated if identifying the modules is confounded by the amplitudes of oscillations of individual nodes of the network. We compared modules identified from 20 subject-level networks of phase synchronization, across frequencies, before and after removing amplitude-related differences in strengths of functional connections. The identified modules were highly similar before and after

539 correcting for amplitude-related differences, across all subjects and frequencies (Figure S6). Hence,
540 the identified modules are not confounded by oscillation amplitudes of individual network nodes.

541 4. Discussion

542 Modules in the fMRI connectome comprise distinct sets of connected regions for sensory, motor and
543 cognitive processing (Valencia et al. (2009), Benjaminsson et al. (2010), Yeo at al. (2011), Power et
544 al. (2011), Lee et al. (2012)). In this study, we investigated whether connectomes of phase-
545 synchronization between fast neuronal oscillations possess modular organization akin to that
546 observed in fMRI connectomes. We used intracerebral SEEG data from 67 subjects to generate
547 connectomes of phase-synchronization between meso-scale cortical oscillations, negligibly affected
548 by volume conduction. We found that connectomes of phase-synchronization possessed modular
549 organization at multiple spatial scales, at all studied frequencies. The modules were anatomically
550 similar within neurophysiologically meaningful frequency bands, *i.e.* delta (3-4 Hz), theta/alpha (5-
551 10 Hz), beta (14-20 Hz), gamma (28-57 Hz), high-gamma (80-113 Hz) and high frequency oscillation
552 (135-320 Hz) bands. In contrast to the modules identified in fMRI, we found that modules up to high-
553 gamma frequency band (80-113 Hz) comprised only anatomically contiguous regions. Importantly,
554 modules comprised brain regions with significantly shared functional roles in *e.g.* attentional and
555 executive function, language and memory.

556 **SEEG recordings can be used to identify modules in connectomes of phase-synchronization**

557 Despite the millimeter scale anatomical specificity and high signal-to-noise ratio (SNR) offered by
558 intra-cranial EEG methods like Electrocorticography and SEEG (Parvizi & Kastner (2018)), their
559 sparse spatial coverage and artefacts due to epileptogenic activity have militated against their use to
560 identify modules in connectomes of phase-synchronization. Our results demonstrate the viability of
561 combining SEEG recordings with state-of-the-art methods to identify modules in connectomes of
562 phase-synchronization. We counteracted sparse SEEG coverage by pooling data from 67 subjects and
563 addressed epileptogenic artefacts by removing SEEG contacts and data segments potentially
564 containing epileptic artefactual activity. Further, we used automated procedures to overcome the
565 problem of assigning SEEG contacts to brain regions and used closest-white-matter referencing to
566 minimise volume conduction, to accurately estimate connectomes of phase-synchronization. Finally,
567 we combined consensus clustering with community detection to identify modules in the connectomes,
568 despite the presence of missing connections. A recent MEG study (Zhigalov et al. (2017)) used a
569 similar procedure with a smaller cohort (N = 27) to estimate the connectome of phase-
570 synchronization, but did not identify modules in these due to the high proportion of missing

connections. A recent Electrocorticography (ECoG) study (Kucyi et al. (2018)) measured amplitude correlations between a number of brain regions, but lacked the spatial coverage to estimate the connectome or modules in the connectome. Hence, our study is the first to our knowledge to harness the high SNR and fine anatomical specificity of intra-cranial EEG to study the modular organization of the connectome of phase-synchronization.

SEEG reveals novel modules in connectomes of phase-synchronization

Some of the distinct modules we identified with SEEG have not previously been observed with non-invasive methods. We identified modules comprising superior frontal regions, inferior frontal regions, superior temporal regions, inferior temporal regions, parietal regions, insula, lateral occipital regions and medial occipital regions. A recent MEG study (Zhigalov et al. (2017)) also reported the presence of modules in occipital, parietal and frontal regions. Another recent MEG study (Vidaurre et al. (2018)) used Hidden-Markov modelling to identify spatially localised "functional states", including those comprising occipital, parietal and frontal regions. The "functional states", were short-lived patterns of inter-regional coherence and hence, constituted module-like structures. However, the modules we identified in superior frontal, inferior frontal, superior temporal, inferior temporal and insula regions are novel to this study. These novel modules might be observed due to the sensitivity of interaction measures, *e.g.* Phase Locking Value, to near-zero-lag phase-synchronization when used with SEEG. MEG field spread or EEG volume conduction produce high amounts of spurious phase-synchronization when these measures are applied to MEG or EEG data.

Similar to the modules we identified with SEEG, modules comprising occipital regions, parietal regions and temporal regions have been identified in resting-state fMRI (Benjaminsson et al. (2010), Yeo et al. (2011), Power et al. (2011)). However, we also identified novel modules comprising regions in the superior frontal, inferior frontal and insula regions. Further, we identified separate modules of superior temporal and inferior temporal regions compared to a single module of temporal regions reported in fMRI, and separate modules of medial occipital and lateral occipital regions compared to a single module of occipital regions reported in fMRI. Each of these modules comprised anatomically contiguous regions in contrast to, for e.g., attentional or default-mode brain systems identified with fMRI, which include regions distributed across frontal, parietal, and temporal lobes (Benjaminsson et al. (2010), Yeo et al. (2011), Power et al. (2011)). Hence, SEEG furnishes novel modules or sets of regions functionally interacting during resting-state.

Modules at multiple spatial scales consistent with hierarchical organization

Our study is the first to report modular organization at multiple spatial scales in connectomes of phase-synchronization. The module of frontal regions identified at a coarse spatial scale splits into modules of superior frontal regions and inferior frontal regions at a finer spatial scale. Similarly, the module of temporal regions identified at a coarse spatial scale splits into modules of superior temporal regions and inferior temporal regions at a finer spatial scale. This recursive occurrence of sub-modules within modules is consistent with hierarchical modular organization, and has been observed in resting-state fMRI (Meunier et al. (2009)) but not with electrophysiological methods. However, a stricter assessment of hierarchical modular organization requires simultaneously identifying modules at multiple spatial scales. Separately identifying modules at multiple spatial scales, as in the current study, make it difficult to rigorously assess hierarchical modular organization due to the very high number of possible permutations when matching modules across spatial scales.

Functional specificity of identified modules suggests their behavioural relevance

We used information from an independent database of fMRI studies to infer the functional role of each module. Regions in different modules had shared involvement in cognitive functions of attention and executive function, affective processing and social cognition, somatosensory processing, language and auditory processing, memory function, visual processing, advanced visual processing and sensori-motor processing respectively. The demonstrated functional specificity of these modules suggests that they operate as distinct brain systems. In line with proposed frameworks on brain function (Tononi et al. (1994), Tononi et al. (1998), Balduzzi & Tononi (2008), Lord et al. (2017), Shine et al. (2018)) strong connections within modules might support segregated information processing (Chan et al. (2014)), while weak connections between modules might support integrated information processing (Deco et al. (2015), Westphal et al. (2017)).

We speculate that the identified modules impose a functional architecture of the connectome during resting-state, which is reorganized to meet task-related demands for segregation and integration. Recent frameworks propose that cognitive function is implemented by integration between modules present in the baseline period (Wig (2017)). Some fMRI studies have found evidence to support this, in the form of associations between cognitive performance and task-related functional reorganization of the brain to facilitate interaction between modules operating at baseline (Spadone et al. (2015), Shine et al. (2016), Cohen & D'Esposito (2016)). While many MEG/EEG studies have found task-related phase synchronization in for e.g. studies of attention (Lobier et al. (2018)), somatosensory processing (Hirvonen et al. (2018)) and working memory (Kitzbichler et al. (2011)),

634 there are no studies investigating task-related phase synchronization as reorganization of the
635 functional architecture imposed by modules during resting-state. Future studies could describe task-
636 related phase-synchronization with reference to the natural framework provided by the identified
637 modules in connectomes of phase-synchronization during resting-state.

638 5. Conclusion

639 In this study, we combined resting-state SEEG recordings with state-of-the-art methods to
640 accurately identify modules in connectomes of phase-synchronization. We found the modules to
641 predominantly comprise anatomically contiguous regions, unlike modules identified in resting-state
642 fMRI. Importantly, each of the modules comprised regions with shared involvement in specific
643 cognitive functions. Hence, these modules might represent distinct brain systems with particular
644 roles in perceptual, cognitive and motor processing.

645 Acknowledgments

646 The authors gratefully acknowledge the support of Human Brain Project (604102), Sigrid Juselius
647 Foundation and Academy of Finland (J.M.P. project numbers: 253130, 256472, 281414, 296304,
648 266745. S.P. project numbers: 266402, 266745, 303933, 325404) to complete this project. Further,
649 the authors are grateful to Jonni Hirvonen and Santeri Rouhinen, for help with data processing, and
650 to Dr. Franceso Cardinale and Annalisa Rubino for facilitating the SEEG recordings.

651 References

652 1. Arenas A., Díaz-Guilera A., Pérez-Vicente C. (2006) Synchronization reveals topological scales
653 in complex networks. *Phys Rev Lett*, 96(11), 114102
654 2. Arnulfo G., Hirvonen J., Nobili L., Palva S., Palva M. (2015a) Phase and amplitude correlations
655 in resting-state activity in human stereotactical EEG recordings. *NeuroImage*, 112:114-127
656 3. Arnulfo G., Narizzano M., Cardinale F., Fato M., Palva M. (2015b) Automatic segmentation of
657 deep intracerebral electrodes in computed tomography scans. *BMC Bioinform*, 16(1):1-12
658 4. Arnulfo G., Wang S., Myrov V., Toselli B., Hirvonen J., Fato M., Nobili L., Cardinale F.,
659 Rubino A., Zhigalov A., Palva S., Palva M. (2020) Long-range phase synchronization of high-
660 frequency oscillations in human cortex. *Nat Commun*, 11:5363
661 5. Balduzzi D., Tononi G. (2008) Integrated Information in Discrete Dynamical Systems:
662 Motivation and Theoretical Framework. *PLoS Comput Biol* 4(6): e1000091

6. Bastos A., Vezoli J., Bosman C., Schoffelen J., Oostenveld R., Dowdall J., De Weerd P., Kennedy H., Fries P. (2015) Visual areas exert feedforward and feedback influences through distinct frequency channels. *Neuron*, 85(2):390-401
7. Beckmann C., DeLuca M., Devlin J., Smith S. (2005) Investigations into resting-state connectivity using independent component analysis. *Philos Trans R Soc Lond B Biol Sci,* 360(1457): 1001-1013
8. Ben-Hur A., Elisseeff A., Guyon I. (2002) A stability based method for discovering structure in the clustered data. *Pac Symp Biocomput*, 6-17
9. Benjamini Y., Hochberg Y. (1995) Controlling the false discovery rate: a practical and powerful approach to multiple testing. *J R Statist Soc B*, 57(1):289-300
10. Benjaminsson S., Fransson P., Lansner A. (2010) A novel model-free data analysis technique based on clustering in a mutual information space: application to resting-state fMRI. *Front Syst Neurosci*, 4:34
11. Blondel V., Guillame J-L, Lambiotte R., Lefebvre E. (2008) Fast unfolding of communities in large networks. *J Stat Mech,* P10008
12. Brookes M., Woolrich M., Barnes G. (2012) Measuring functional connectivity in MEG: a multivariate approach insensitive to linear source leakage. *NeuroImage*, 63(2):910-920
13. Brookes M., Woolrich M., Luckhoo H., Price D., Hale J., Stephenson M., Barnes G., Smith S., Morris P. (2011) Investigating the electrophysiological basis of resting state networks using magnetoencephalography. *Proc Natl Acad Sci USA,* 108(40):16783-16788
14. Cohen J., D'Esposito M. (2016) The segregation and integration of distinct brain networks and their relationship to cognition. *J Neurosci*, 36(48):12083-12094
15. da Silva F. (2011) EEG and MEG: Relevance to Neuroscience. *Neuron*, 80(5):1112-1128
16. Damoiseaux J., Rombouts S., Barkhof F., Scheltens P., Stam C., Smith S, Beckmann C. (2006) Consistent resting-state networks across healthy subjects. *Proc Natl Acad Sci USA*, 103(37):13848-13853
17. Deco G., Tononi G., Boly M., Kringelbach M. (2015) Rethinking segregation and integration: contributions of whole-brain modelling. *Nat Rev Neurosci*, 16(7): 430-439
18. Destrieux C., Fischl B., Dale A., Halgren E. (2010) Automatic parcellation of human cortical gyri and sulci using standard anatomical nomenclature. *NeuroImage*, 53(1):1-15
19. Doucet G., Naveau M., Petit L., Delcroix N., Zago L., Crivello F., Jobard G., Tzourio-Mazoyer N., Mazoyer B., Mellet E., Joliot M. (2011) Brain activity at rest: a multiscale hierarchical functional organization. *J Neurophysiol*, 105(6):2753-2763

20. Engel A., Gerloff C., Hilgetag C., Nolte G. (2013) Intrinsic coupling modes: multiscale interactions in ongoing brain activity. *Neuron*, 80(4):867-886
21. Fell J., Axmacher N. (2011) The role of phase synchronization in memory processes. *Nat Rev Neurosci,* 12 (2): 105-118
22. Fries P. (2015) Rhythms for cognition: communication through coherence. *Neuron*, 88(1):220-235
23. Gazzaniga, M., Ivry, R. and Mangun, G. (2009) Cognitive Neuroscience: The Biology of the Mind. Norton Press, London
24. Hirvonen J, Monto S, Wang S, Palva M, Palva S (2018) Dynamic large-scale network synchronization from perception to action. *Netw Neurosci*, 2(4):442-463
25. Kitzbichler M., Henson R., Smith M., Nathan P., Bullmore E. (2011) Cognitive effort drives workspace configuration of human brain functional networks. *J Neurosci*, 31(22):8259-8270
26. Kucyi A., Schrouff J., Bickel S., Foster B., Shine J., Parvizi J. (2018) Intracranial electrophysiology reveals reproducible intrinsic functional connectivity with human brain networks. *J Neurosci*, 38(17): 4230-4242
27. Lachaux J-P., Rodriquez E., Martinerie J., Varela F. (1999) Measuring phase synchrony in brain signals. *Hum Brain Mapp*, 8:194-208
28. Lancichinetti A., Fortunato S. (2012) Consensus clustering in complex networks. *Sci Rep*, 2(1):1-7
29. Lee M., Hacker C., Snyder A., Corbetta M., Zhang D., Leuthardt E. (2012) Clustering of resting state networks. *PLoS ONE*, 7(7): e40370
30. Lobier M, Palva M, Palva S (2018) High-alpha band synchronization across frontal, parietal and visual cortex mediates behavioural and neuronal effects of visuospatial attention. *NeuroImage*, 165:222-237
31. Lord L., Stevner A., Deco G., Kringelbach M. (2017) Understanding principles of integration and segregation using whole-brain computational connectomics: implications for neuropsychiatric disorders. *Phil Trans R Soc A* 375: 20160283
32. Meunier D., Lambiotte R., Fornito A., Ersche K., Bullmore E. (2009) Hierarchical modularity in human brain functional networks. *Front Neuroinformatics*, 3:37
33. Mucha P., Richardson T., Macon K., Porter M., Onnela J-P. (2010) Community structure in time-dependent, multiscale and multiplex networks. *Science*, 328(5980):876-878
34. Narizzano M., Arnulfo G., Ricci S., Toselli B., Tisdall M., Canessa A., Cardinale F. (2017) SEEG assistant: a 3DSlicer extension to support epilepsy surgery. *BMC Bioinform*, 18:124

729 35. Palva M., Palva S., Kaila K. (2005) Phase synchrony among neuronal oscillations in the human
730 cortex. *J Neurosci*, 25(15): 3962-3972
731 36. Palva M., Wang S., Palva S., Zhigalov A., Monto S., Brookes M., Schoffelen J., Jerbi K. (2018)
732 Ghost interactions in MEG/EEG source space: A note of caution on inter-areal coupling
733 measures. *NeuroImage*, 173:632-643
734 37. Palva S., Palva M. (2012) Discovering oscillatory interaction networks with M/EEG: challenges
735 and breakthroughs. *Trends Cogn Sci*, 16(4): 219-230
736 38. Parvizi J., Kastner S. (2018) Promises and limitations of human intracranial
737 electroencephalography. *Nat Neurosci*, 21(4):474-483
738 39. Power J., Cohen A., Nelson S., Wig G., Barnes K., Church J., Vogel A., Laumann T., Miezin
739 F., Schlaggar B., Petersen S. (2011) Functional network organization of the human
740 brain. *Neuron*, *72*(4): 665-678
741 40. Reichardt J., Bornholdt S. (2006) Statistical mechanics of community detection. *Phys Rev E*,
742 74(1),016110
743 41. Ronhovde P., Nussinov Z. (2009) Multiresolution community detection for megascale networks
744 by information-based replica correlations. Phys Rev E, 80(1), 016109
745 42. Rosvall M., Bergstrom C. (2008) Maps of random walks on complex networks reveal
746 community structure. *Proc Natl Acad Sci USA*, 105(4):1118-1123
747 43. Rubinov M., Sporns (2010) Complex network measures of brain connectivity: Uses and
748 interpretations. *NeuroImage*, 52(3):1059-1069
749 44. Schroeder C., Lakatos P. (2009) Low-frequency neuronal oscillations as instruments of sensory
750 selection. *Trends Neurosci.* 32(1):9-18
751 45. Shine J., Aburn M., Breakspear M., Poldrack R. (2018) The modulation of neural gain
752 facilitates a transition between functional segregation and integration in the brain. *eLife*,
753 7:e31130
754 46. Shine J., Bissett P., Bell P., Koyejo O., Balsters J., Gorgolewski K., Moodie C., Poldrack R.
755 (2016) The dynamics of functional brain networks: integrated network states during cognitive
756 task performance. *Neuron*, 92:544-554
757 47. Smith S., Fox P., Miller K., Glahn D., Fox M., Mackay C., Filippini N., Watkins K., Toro R.,
758 Laird A., Beckmann C. (2009) Correspondence of the brain's functional architecture during
759 activation and rest. *Proc Natl Acad Sci USA*, 106(31):13040-13045
760 48. Spadone S., Penna S., Sestieri C., Betti V., Tosoni A., Perrucci M., Romani G., Corbetta M.
761 (2015) Dynamic reorganization of human resting-state networks during visuospatial attention.
762 *Proc Natl Acad Sci USA,* 112(26): 8112-8117

763 49. Sun Y., Danila B., Josić K, Bassler K (2009) Improved community structure detection using a
764 modified fine-tuning strategy. *EPL Europhys Lett*, 86(2), 28004
765 50. Tononi G., Edelman G., Sporns O. (1998) Complexity and coherency: integrating information
766 in the brain. *Trends Cogn Sci*, 2(12): 474-484
767 51. Tononi G., Sporns O., Edelman G. (1994) A measure for brain complexity: relating functional
768 segregation and integration in the nervous system. *Proc Natl Acad Sci USA,* 91(11):5033-5037
769 52. Uhlhaas P., Roux F., Rodriguez E., Rotarska-Jagiela A., Singer W. (2010) Neural synchrony
770 and the development of cortical networks. *Trends Cogn Sci*, 14(2):72-80
771 53. Valencia M., Pastor M., Fernández-Seara M., Artieda J., Martinerie J., Chavez M. (2009)
772 Complex modular structure of large-scale brain networks. *Chaos*, 19(2):023119
773 54. van den Heuvel M., Pol H. (2010) Exploring the brain network: a review on resting-state fMRI
774 functional connectivity. *Eur Neuropsychopharmacol*. 20(8):519-534
775 55. Vanhatalo S., Palva M., Holmes M., Miller J., Voipio J., Kaila K. (2004) Infraslow oscillations
776 modulate excitability and interictal epileptic activity in the human cortex during sleep. *Proc*
777 *Natl Acad Sci USA,* 101(14):5053-5057
778 56. Varela F., Lachaux J., Rodriguez E., Martinerie J. (2001) The brainweb: phase-synchronization
779 and large-scale integration. *Nat Rev Neurosci*, 2(4):229-239
780 57. Vidaurre D., Hunt L., Quinn A., Hunt B., Brookes M., Nobre A., Woolrich M. (2018)
781 Spontaneous cortical activity transiently organizes into frequency-specific phase-coupling
782 networks. *Nat Commun*, 9:2987
783 58. Vinck M., Oostenveld R., Wingerden M., Battaglia F., Pennartz C. (2011) An improved index
784 of phase-synchronization for electrophysiological data in the presence of volume-conduction,
785 noise and sample-size bias. *NeuroImage*, 55(4):1548-1565
786 59. Westphal A., Wang S., Rissman J. (2017) Episodic Memory Retrieval Benefits from a Less
787 Modular Brain Network Organization. *J Neurosci*, *7(13):3523-3531*
788 60. Wig G (2017) Segregated systems of human brain networks. *Trends Cogn Sci*, 21(12): 981-996
789 61. Williams N., Arnulfo G., Wang S., Nobili L., Palva S., Palva M. (2019) Comparison of methods
790 to identify modules in noisy or incomplete brain networks. *Brain Connect*, 9(2):128-143
791 62. Williams N., Wang S., Arnulfo G., Nobili L., Palva S., Palva M. (2021) Modules in Human
792 Electrophysiological Connectomes of Phase-Synchronization. *Mendeley Data*, V1
793 63. Yarkoni T., Poldrack R., Nichols T., Van Essen D., Wager T. (2011) Large-scale automated
794 synthesis of human functional neuroimaging data. *Nat Methods*, 8(8):665-670
795 64. Yeo B., Krienen F., Sepulchre J., Sabuncu M., Lashkari D., Hollinshead M., Roffman J.,
796 Smoller J., Zöllei L, Polimeni J., Fischl B., Liu H., Buckner R. (2011) The organization of the

human cerebral cortex estimated by intrinsic functional connectivity. *J Neurophysiol*, 106(3): 1125-1165

65. Zhigalov A., Arnulfo G., Nobili L., Palva S., Palva M. (2015) Relationship of fast-and-slow-timescale neuronal dynamics in human MEG and SEEG. *J Neurosci*, 35(13):5385-5396
66. Zhigalov A., Arnulfo G., Nobili L., Palva S., Palva M. (2017) Modular co-organization of functional connectivity and scale-free dynamics in the human brain. *Netw Neurosci* 1(2):143-165

Supplementary figures

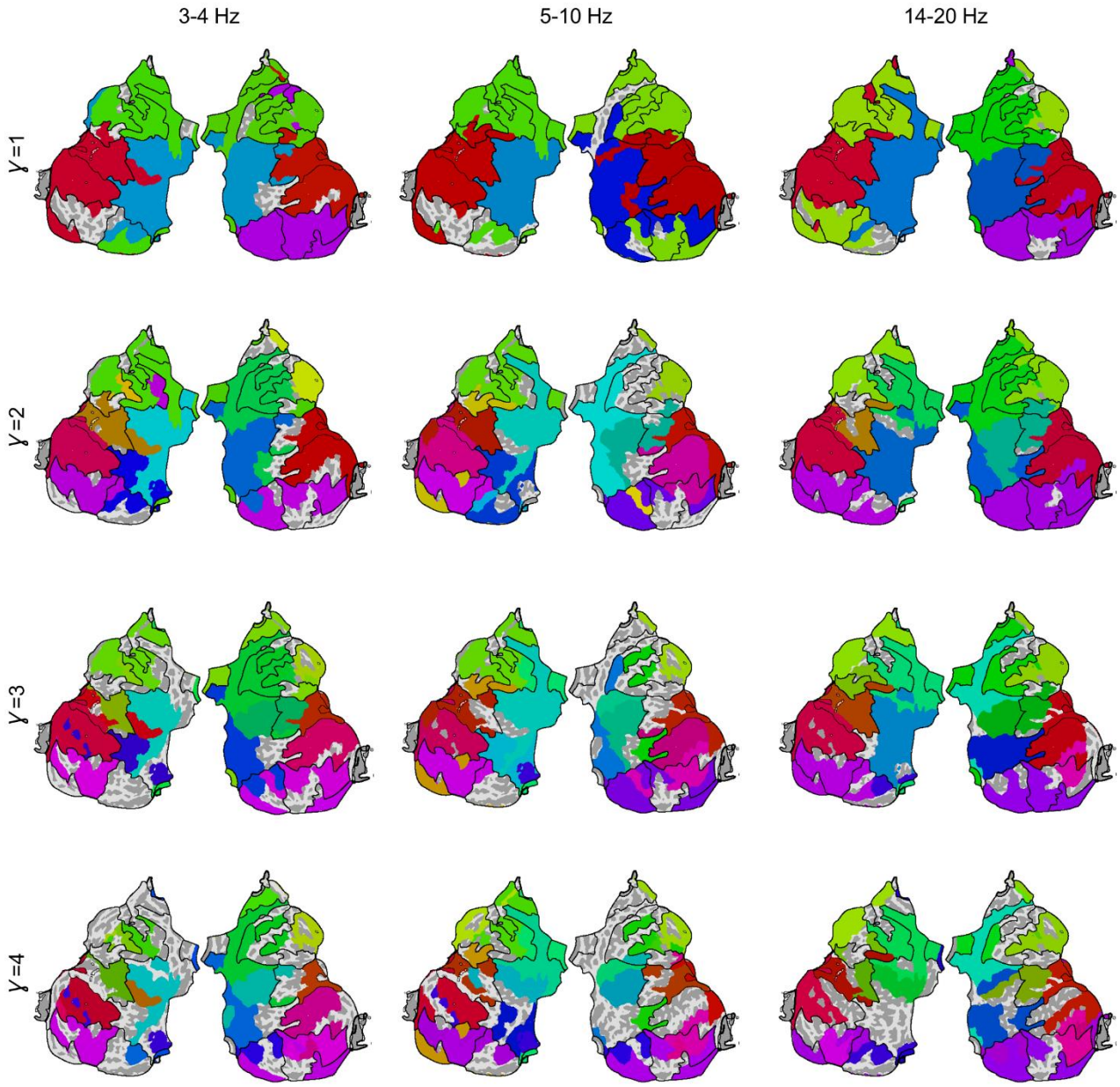

Figure S1. Modules in connectomes of phase-synchronization for 3-4 Hz, 5-10 Hz and 14-20 Hz comprise anatomically contiguous regions. Flat-brain representations of modules in connectomes of phase-synchronization for 3-4 Hz, 5-10 Hz and 14-20 Hz, at four spatial scales (γ = 1 to 4). Black lines on each flat-brain show outlines of consensus modules, *i.e.* sets of regions assigned to the same module across frequencies and spatial scales.

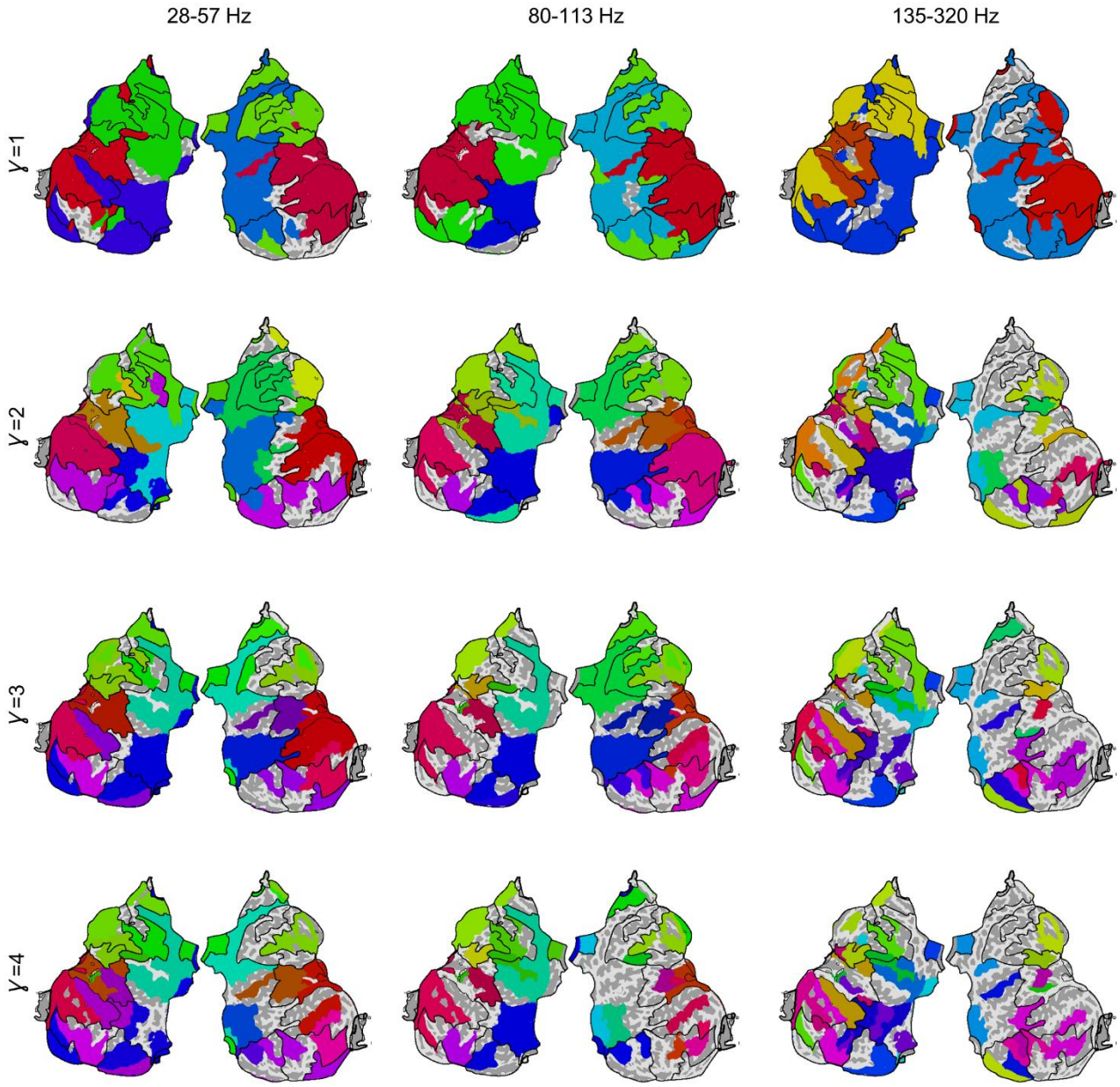

Figure S2. Modules in connectomes of phase-synchronization for 28-57 Hz, 80-113 Hz but not 135-320 Hz comprise anatomically contiguous regions. Flat-brain representations of modules in connectomes of phase-synchronization for 28-57 Hz, 80-113 Hz and 135-320 Hz, at four spatial scales (γ = 1 to 4). Black lines on each flat-brain show outlines of consensus modules, *i.e.* sets of regions assigned to the same module across frequencies and spatial scales.

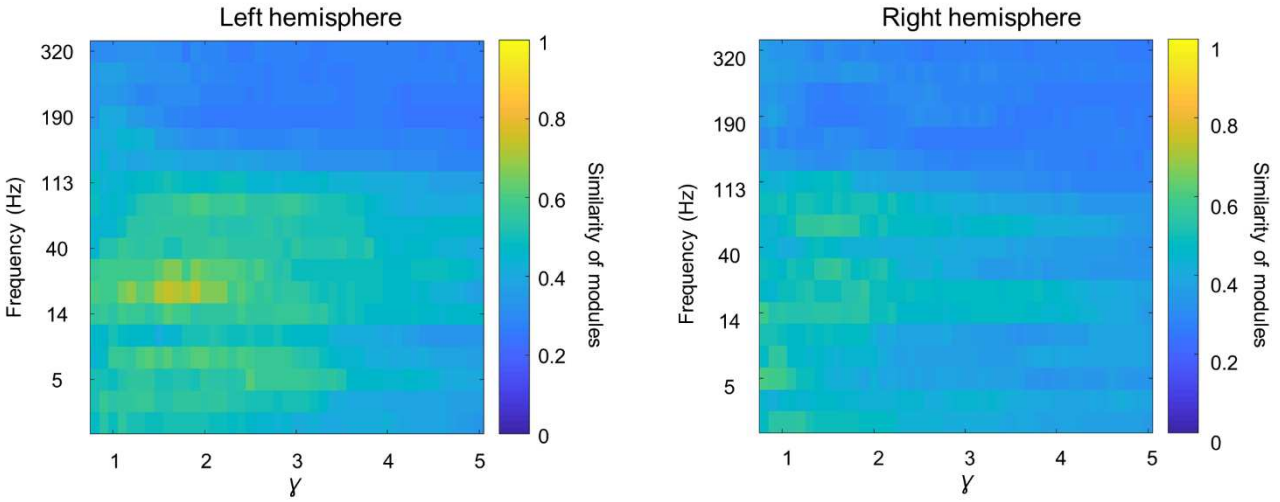

Figure S3. Consensus modules resemble modules at lower frequencies and intermediate spatial scales. Similarity between consensus modules and modules at each combination of spatial scale and frequency, for both left and right hemispheres.

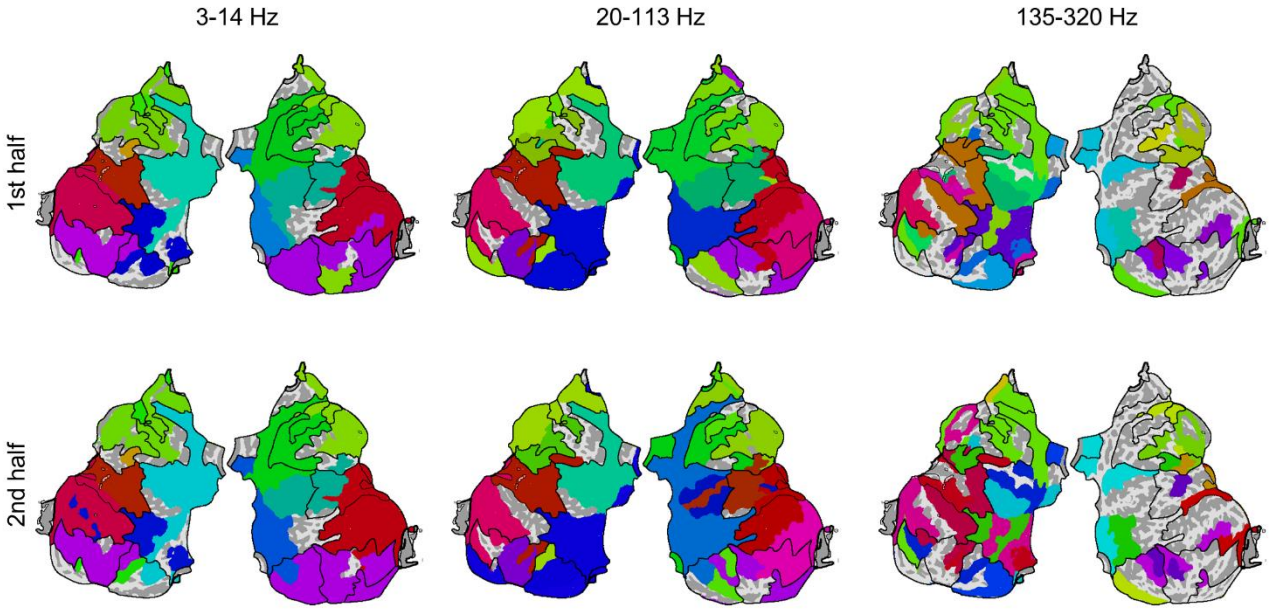

Figure S4. Modules in split connectomes of phase-synchronization are highly similar. Flat-brain representations of modules in two split connectomes of phase-synchronization (top and bottom rows) for 3-14 Hz, 20-113 Hz and 135-320 Hz, at a single spatial scale ($\gamma = 2$). Black lines on each flat-brain show outlines of consensus modules, *i.e.* sets of regions assigned to the same module across frequencies and spatial scales.

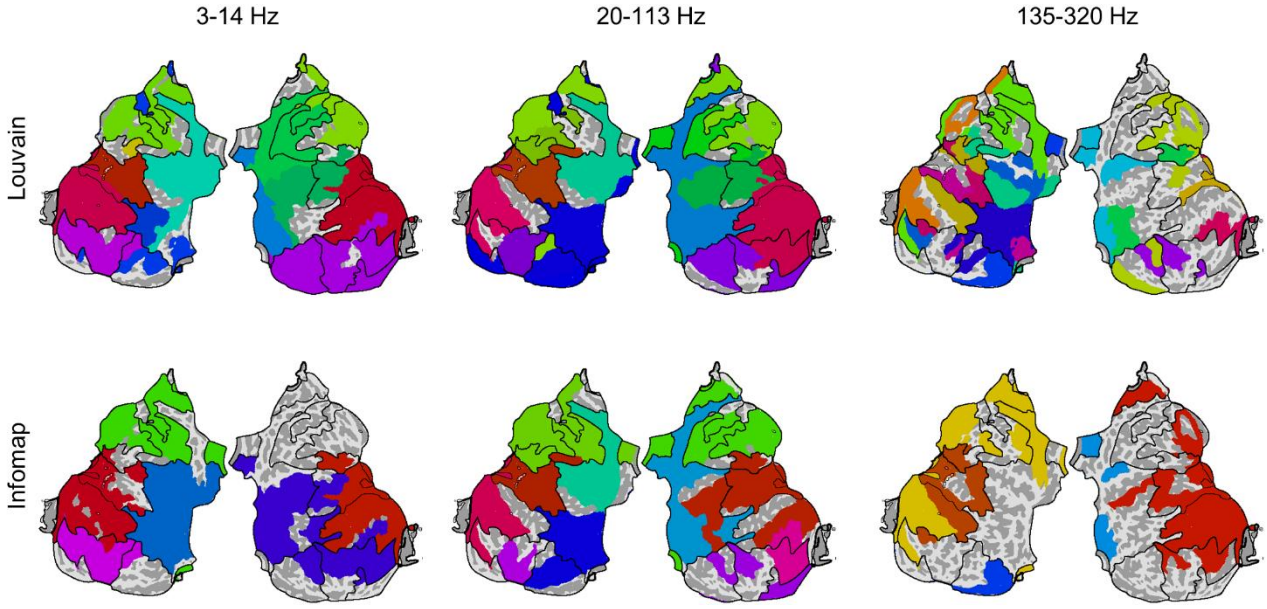

Figure S5. Modules in connectomes of phase-synchronization similar for Louvain and Infomap community detection, up to high gamma frequency band. Flat-brain representations of modules in connectomes of phase-synchronization estimated with Louvain (top row) and Infomap (bottom row) community detection, for 3-14 Hz, 20-113 Hz and 135-320 Hz, at a single spatial scale ($\gamma = 2$). Black lines on each flat-brain show outlines of consensus modules, *i.e.* sets of regions assigned to the same module across frequencies and spatial scales.

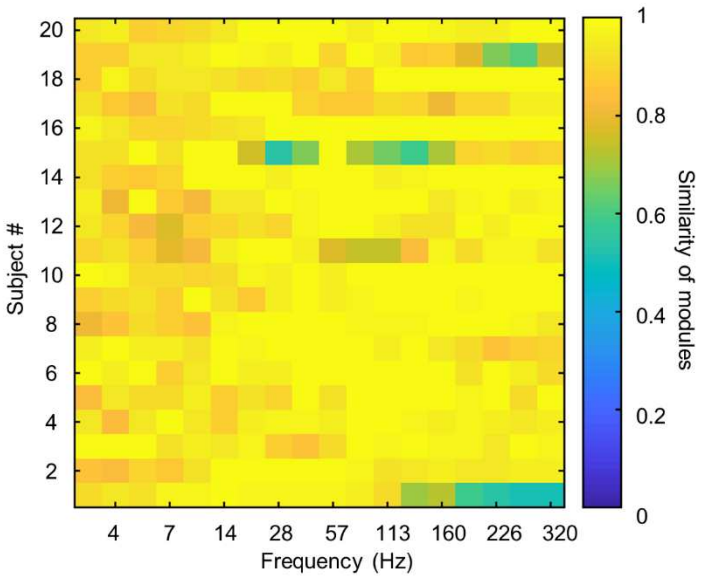

908

909 **Figure S6. Amplitude of activity does not confound identification of modules.** Similarity
910 between modules identified on subject-level networks of phase-synchronization before and after
911 removing amplitude confound.

912

913

914

915

916

917